



This is the accepted manuscript made available via CHORUS, the article has been published as:

Theoretical Tracking of Resonance-Enhanced Multiple Ionization Pathways in X-ray Free-Electron Laser Pulses/article-title>

Phay J. Ho, Christoph Bostedt, Sebastian Schorb, and Linda Young

Phys. Rev. Lett. **113**, 253001 — Published 18 December 2014

DOI: [10.1103/PhysRevLett.113.253001](https://doi.org/10.1103/PhysRevLett.113.253001)

Theoretical tracking of resonance-enhanced multiple ionization pathways in XFEL pulses

Phay J. Ho¹, Christoph Bostedt², Sebastian Schorb² and Linda Young¹

¹*Argonne National Laboratory, Argonne, Illinois 60439, USA and*

²*Linac Coherent Light Source, SLAC National Accelerator Laboratory, Stanford, California 94309, USA*

(Dated: November 14, 2014)

We present an extended Monte Carlo rate equation (MCRE) approach to examine the inner-shell ionization dynamics of atoms in an intense x-ray free-electron laser (XFEL) pulse. In addition to photoionization, Auger decay and fluorescence processes, we include bound-to-bound transitions in the rate equation calculations. Using an efficient computational scheme, we account for “hidden resonances” unveiled during the course of an XFEL pulse. For Ar, the number of possible electron configurations is increased 10 billion-fold over that required under non-resonant conditions. We investigated the complex ionization dynamics of Ar atoms exposed to an 480-eV XFEL pulse, where production of ions above charge-state 10+ is not allowed via direct one-photon ionization. We found that resonance-enhanced x-ray multiple ionization (REXMI) pathways play a dominant role in producing these nominally inaccessible charge states. Our calculated results agree with the measured Ar ion yield and pulse-duration dependence. The MCRE method enables theoretical exploration of the complex dynamics of resonant high-intensity x-ray processes.

PACS numbers: 32.80.Rm, 41.60.Cr, 02.70.Uu

Hard x-ray free-electron laser (XFEL) pulses, currently available at the Linac Coherent Light Source (LCLS) [1] and SACLA [2], provide unprecedented opportunities to image complex systems with atomic resolution [3] on ultrafast timescales. Free-electron-laser imaging of complex systems relies on the diffract-before-destroy concept, where a single high-fluence, ultrashort x-ray pulse yields a diffraction pattern prior to Coulomb explosion and reconstruction of many such patterns will render a 3D model [4, 5]. Given that the diffraction pattern is generated by photon scattering from the electron distribution, and that massive electronic rearrangement occurs within the femtosecond x-ray pulse [6], it is of fundamental interest to obtain a deep understanding of the dynamical electronic response of individual atoms to intense x-ray pulses.

Considerable efforts have been devoted to the study of ionization of atoms exposed to high-fluence, high-intensity XFEL pulses [6–12]. Early studies of atomic Ne demonstrated clearly that the dominant ionization mechanism under focused XFEL conditions ($\sim 10^{12}$ photons/ μm^2 /50-fs pulse) is sequential single-photon absorption [6], and that the contribution of the direct, i.e. non-sequential, two-photon process is very small [7]. In these experiments on Ne, and analogous ones in the hard x-ray regime on Xe [12], the highest observed charge state is that energetically accessible by one-photon ionization. For these cases with XFEL photon energies far from resonances, a rate equation model [13, 14], reproduces experimental observations. However, high-fluence XFEL pulses can reveal “hidden” resonances, i.e. bound-bound transitions not present in the original target atom ground state; such resonances can dramatically enhance ionization pathways as resonant exceed non-resonant cross-sections by many orders of magnitude [8].

Ultraefficient ionization through resonance enhance-

ment was recently discovered in XFEL experiments on atomic Xe [9] and Kr [10]. In Xe and Kr, at photon energies of 1.5 keV and 2.0 keV respectively, charge states well beyond those accessible via single-photon ionization were observed. Rudek and coworkers showed that a rate equation model without resonant excitation fails to account for the appearance of Xe charge states from 27+ to 36+ and Kr charge states higher than 15+ by many orders of magnitude [9, 10]. To explain the observed discrepancies, they proposed the resonance-enhanced x-ray multiple ionization (REXMI) mechanism, where excitation of multiple electrons into outer valence and Rydberg orbitals is followed by autoionization to produce extremely high charge states. Similarly, Schorb and coworkers [15] suggested that the surprising appearance of Ar¹¹⁺ at a photon energy of 480 eV was due to resonances. The importance of resonances in multiple ionization of valence-shell electrons of Ar has also been studied using extreme ultraviolet (EUV) radiation [16, 17] where, relative to x-ray studies, the number of electronic configurations involved is small.

Despite the large body of experimental evidence and its clear importance, the role of resonant excitation has not been fully incorporated in theoretical models for x-ray ionization. The computational problem is severe because the number of electronic configurations (ECs) increases exponentially when one or more resonant excitations are allowed. For Ar, the number of accessible ECs for the 5 occupied subshells (1s to 3p) to produce charge state from 0 to 18 is 1323 [18]. Here each subshell can have 0 to its maximum occupancy of $2(2l + 1)$, where l is the its angular momentum. However, when resonant excitations are allowed, one or more electrons can occupy subshells beyond 3p. To include orbitals with quantum number $n = 0$ to 10 and $l = 0$ to 3, the number of ECs will increase to more than 2.85×10^{13} . The need to include all

the possible ECs clearly presents a daunting computational challenge for the standard rate equation approach, where more than 2.85×10^{13} coupled rate equations would need to be solved using a huge predetermined table containing all the relevant cross sections and decay rates. Because of this daunting challenge, previous attempts to treat resonances [19, 20] were limited to *single* resonant excitation channels in Ne systems.

Here we present a Monte Carlo computational scheme that includes bound-bound resonant excitations comprehensively for the first time. We use this scheme to validate the role of the REXMI mechanism in the production of high charge states from atomic Ar exposed to an intense XFEL pulse and to explain the pulse-duration dependence of experimental ion yields [21]. We further validate the dramatic role of resonant effects in XFEL ionization of Xe and Kr atoms [9, 10].

Our scheme is similar to the Monte Carlo rate equation (MCRE) method of Son and co-workers [14] that was used to study the response of Ar [22], Kr [10] and Xe [9, 12, 14, 22] atoms in XFEL pulses without including resonant bound-bound excitation. Briefly in the MCRE method, the response of an ensemble of atoms with the same starting electronic configuration is tracked throughout an XFEL pulse. For each atom, its response is characterized as a time series of electronic transitions. At each time step, a random number is generated to determine whether an electronic transition will take place. The probability of a transition being selected is weighted

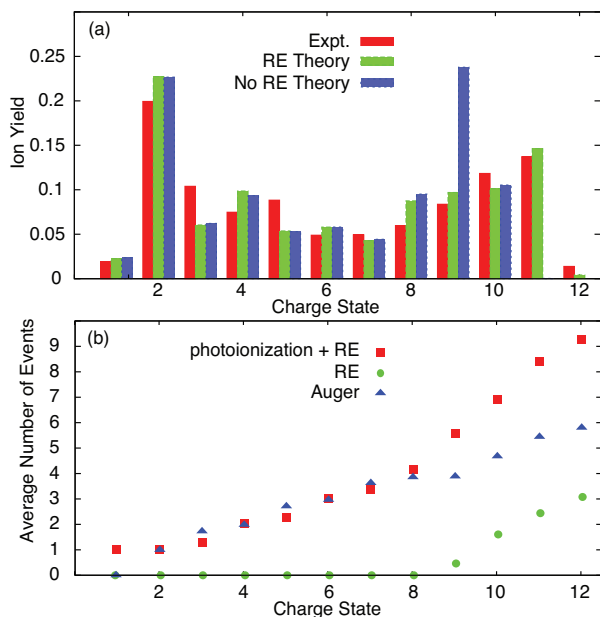


FIG. 1. (Color online) (a) Experimental argon charge state distribution for 50 fs, 0.15 mJ pulses at 480 eV photon energy, resonant-excitation (RE) and no-resonant-excitation (No RE) theory. (b) Average number of absorbed photons, resonant excitation and Auger events predicted by the RE theory.

by its transition strength, which is its transition rate multiplied by the chosen time step size. If an electronic transition occurs, the atom will have a new electronic configuration. This procedure is then repeated until the atom has no more decay channels. Various observables, like the ion yield and statistical data of each type of electronic transition, can be constructed from the responses of an ensemble of realizations. Since each electronic transition is treated as an independent, random event, an adaptive time stepping approach is usually used to speed up the computation. With this MCRE method, the effects of spatiotemporal x-ray beam profile can be studied easily.

We extend the MCRE method to include resonant excitation by having an efficient way to obtain and manage the required atomic data (decay rates, photoabsorption and ionization cross-sections). Rather than computing all the atomic data [9] for all the possible ECs, which is impossible if resonant excitation is included, we compute only the required atomic data at each time step [12]. These are stored in a compact database to speed up the calculation. The number of important ECs depends strongly on the pulse parameters and will grow with higher photon fluence and larger bandwidth. For the calculations presented here on Ar, several thousand ECs are sufficient to capture the atomic response. The power of this method is that it provides a natural and efficient way to select the most probable ECs out of the tens of quadrillions of ECs, calculate the weights of the responsible electronic transitions that connect ECs, and eventually identify the detailed ionization mechanisms.

The atomic response in the XFEL pulse is described using the Hartree-Fock-Slater (HFS) model [23]. Using the numerical grid methods similar to that of the XATOM toolkit [24], we compute the needed photoionization cross sections, resonant excitation cross-sections, Auger and Coster-Kronig and fluorescence rates. We verify the validity of our numerical code by reproducing results from XATOM, i.e. the Ar ion yield at 5 keV [22] and the decay rates and photoionization cross sections in carbon at 8 and 12 keV [24]. We also calculated lifetimes that agree with available experimental data on Ar Rydberg states, $3s3p^64p$ and $3s3p^65p$ [25, 26].

To treat resonant excitation, we include only electric dipole transitions, and allow resonantly excited atoms/ions to undergo further sequential, multiple resonant excitation in addition to photoionization and inner-shell decay. An electron can undergo resonant excitation from a lower state j to an upper state i when the difference between the incident photon energy, ω_X , and the transition energy, $\Delta E_{i,j}$, is within the bandwidth of the XFEL pulse, $\delta\omega$, and the resonant cross section is given

$$\sigma_{RE}(i,j) = \begin{cases} \frac{2\pi^2\alpha}{\delta\omega} f_{i,j}, & \text{if } |\Delta E_{i,j} - \omega_X| \leq \delta\omega \\ 0, & \text{if } |\Delta E_{i,j} - \omega_X| > \delta\omega, \end{cases} \quad (1)$$

where α is the fine structure constant and $f_{i,j}$ is the absorption oscillator strength. We assume the linewidths of the resonant states to be smaller than the bandwidth

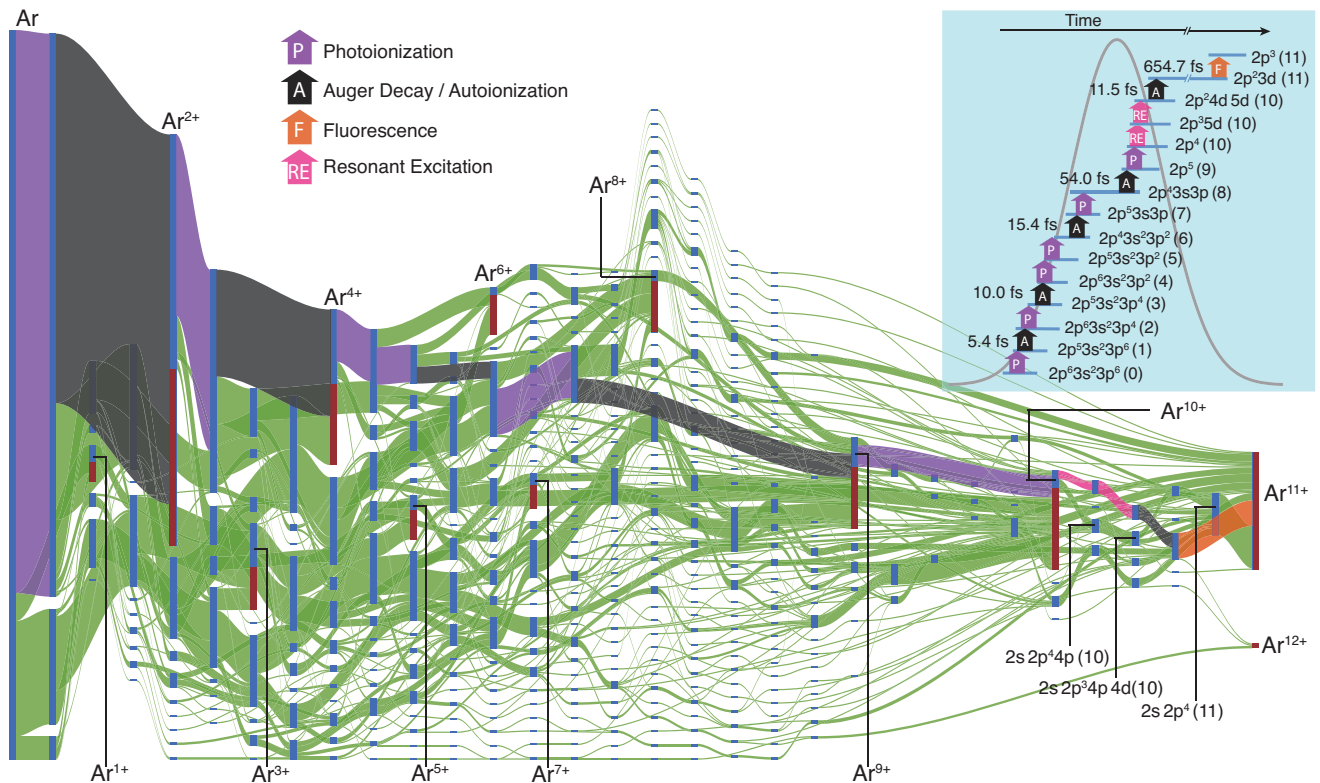


FIG. 2. (Color online) A Sankey diagram illustrating transition probabilities between the accessible ECs of an Ar atom exposed to an intense XFEL pulse at 480-eV. In this diagram, the vertical bars represent ECs, and the width of each green branch, going from left to right, indicates the transition probability between two ECs. Some ECs are transients that do not survive (dark blue bars). The EC fractions that survive are colored red and are ground state ECs. The branches that are not green correspond to a prominent pathway to reach Ar^{11+} from neutral Ar. The branch color is explained in the legend. The inset gives the responsible ECs for this prominent path which accounts for $\sim 10\%$ of the Ar^{11+} yield. The charge state is shown in parentheses and lifetime to left of the arrow. Another prominent pathway to Ar^{11+} that involves multiple resonant excitation is shown by the three labelled ECs with a $2s$ hole.

of the pulse, as is reasonable for the cases here since the XFEL bandwidth ($\sim 5\text{eV}$) is generally much larger than the meV linewidths of Rydberg states [25, 26]. Eq. (1) is obtained by assuming a flat-top XFEL bandwidth profile. The results change by $< 3\%$ for a Gaussian bandwidth profile.

We examine the role of resonant excitation in Ar by performing two sets of calculations: no-resonant-excitation (No RE) theory, with all resonances turned off, and resonant-excitation (RE) theory that include resonances within a given bandwidth. We integrate over the three-dimensional interaction volume defined by the Gaussian spatial beam and gas jet profile. We used a Gaussian temporal beam profile that matched the experimental peak fluence. For each calculation, 10^5 to 10^6 Monte Carlo realizations were used to simulate the atomic response.

Figure 1(a) shows the experimental data (red bars) measured for Ar atoms exposed to 480-eV, 50-fs, 0.15 mJ XFEL pulses with 1 % bandwidth [15, 21]. Assuming a $1.6 \mu\text{m}^2$ x-ray focus and 20% beamline transmis-

sion, this corresponds to a peak fluence of $10 \mu\text{J} \mu\text{m}^{-2}$ achieved within the vicinity of an $100\text{-}\mu\text{m}$ Ar gas jet. The majority of atoms lie outside of the x-ray focus and are exposed to much lower fluence. As a result, it is not surprising that Ar^{2+} is the most abundant ion, produced via L-shell photoionization of neutral Ar followed by Auger decay. The surprising feature is the substantial fraction of Ar^{11+} , 14%, despite the fact that the ionization energy for Ar^{10+} (539 eV) exceeds the photon energy of 480 eV.

The predicted ion yield from the RE theory reproduces the experimental data well. Both reveal a maximum at Ar^{2+} and give comparable yield at Ar^{11+} . The slight discrepancies are mainly due to the HFS model used and omission of other processes, e.g. shake processes and double Auger decay. In contrast, the No RE theory deviates significantly from experiment; the ion yield maximizes at Ar^{9+} and essentially no Ar^{11+} ($< 0.03\%$) is found.

By examining the history of all atoms, we extract statistical information. Figure 1(b) shows that both the average number of photoionization and Auger events increase linearly with the charge state. Interestingly, res-

onant excitation plays an significant role in the production of high charge states beginning as low as Ar^{9+} , and multiple resonant excitation steps may be involved. For example, to reach Ar^{11+} a neutral atom on average will undergo 5 to 6 Auger decays and absorb 8 to 9 photons with 2 to 3 resonant excitations.

These statistical data, however, do not pinpoint the actual REXMI mechanisms. To illustrate the important participating ECs and the weight of each electronic transition, we construct a Sankey diagram [27] in Fig. 2. Clearly, XFEL dynamics in an atom is very complex, involving excited transient states with one or more inner-shell holes and/or one or more electrons in valence shells. Some of the ECs serve as gateways to many other ECs. Given that lifetimes of ECs vary substantially there are many possible pathways, each with a different timescale, that may produce each charge state of Ar.

Figure 2 illustrates sequences of transitions that produce the ground state of Ar^{11+} and highlights that REXMI is responsible. One prominent pathway to Ar^{11+} involves two consecutive resonant excitations followed by an autoionization event to remove an additional electron from the ground state of Ar^{10+} . The first resonant excitation promotes a $2p$ electron to the $5d$ orbital, and creates an excited EC of $1s^2 2s^2 2p^2 5d$ (lifetime > 4 ps) with no Auger decay channel. This long-lived EC has a resonance at 480 eV, enabling excitation of a $2p$ electron to the $4d$ orbital to form a doubly-excited Ar^{10+} ion with EC of $1s^2 2s^2 2p^2 4d 5d$ which autoionizes to $1s^2 2s^2 2p^2 3d$ in 11.5 fs. Fluorescence then brings Ar^{11+} to its ground state. Another prominent pathway to Ar^{11+} that involves doubly resonant excitation is labelled in Fig. 2. Here, two

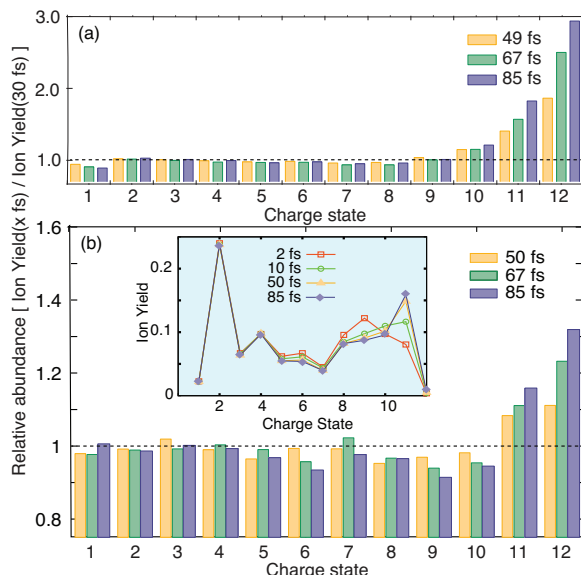


FIG. 3. (Color online) Pulse duration dependence of Ar ion production. (a) Experiment, abundance normalized to value for 30-fs pulse. (b) RE theory. Inset shows absolute yield of Ar ions calculated for different pulse durations.

consecutive resonant excitations of $2s \rightarrow 4p$ and $2p \rightarrow 4d$ promote the ground state of Ar^{10+} to an autoionizing state of $1s^2 2s 2p^3 4p 4d$. Autoionization followed by fluorescence produces ground state Ar^{11+} .

Schorb *et al.* also investigated the pulse duration dependence of the Ar charge state yield (2 mJ and 30, 49, 67 and 85 fs pulses; pulse duration measured to $\sim 10\%$ precision) [21]. Figure 3(a), shows that the ion yield increases with increasing pulse duration for charge states above 10+, whereas the lower charge states show lesser pulse duration dependence. This is a manifestation of induced transparency/frustrated absorption [6, 15, 28, 29] ostensibly due to the bottleneck of multiple Auger decays with long femtosecond lifetimes to reach charge states of 11+ and higher. Figure 3(b) shows that RE theory gives a qualitative trend similar to experiment.

To gain better insight into the pulse duration phenomenon, we extended the calculation to durations of 2 to 85 fs, as shown in the inset of Fig. 3(b). The pulse duration dependence is rather complex. In the case of Ar^{11+} , the calculated ion yield increases with increasing pulse duration, in agreement with experiment. Interestingly the yield of Ar^{11+} is substantial (7%) for a 2-fs pulse even though the path includes multiple Auger decays with a cumulative lifetime of 100 femtoseconds, suggesting that resonant-excitation pathways efficiently select early Auger events. The opposite trend is found for Ar^{9+} , a transient gateway to higher charge states. For Ar^{10+} , the pulse duration dependence is more complicated with reversing trends.

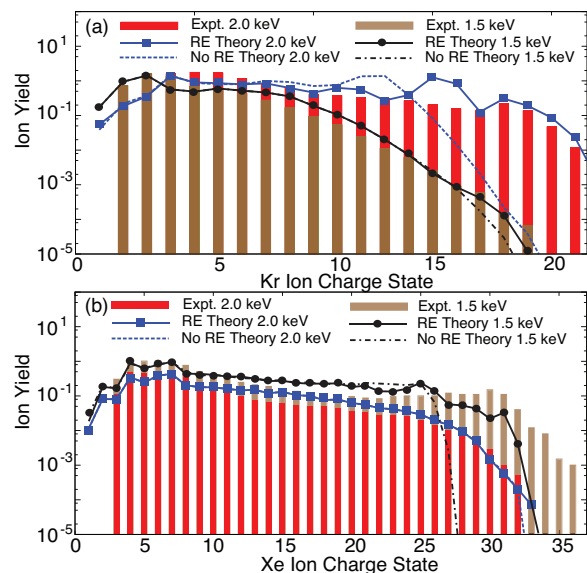


FIG. 4. (Color online) Experimental (a) krypton and (b) xenon charge state distribution (bars) obtained at photon energies of 2.0 keV and 1.5 keV and comparison to resonant-excitation (RE) and no-resonant-excitation (No RE) theory (lines with circles and dash lines) calculated with similar experimental pulse parameters [9, 10].

Finally, we used our MCRE theory to examine previously published Kr and Xe data [9, 10]. Figure 4 shows the comparison of the experimental charge state distribution of krypton [10] and xenon [9] with the prediction from both the No-RE and RE theory at 1.5 keV and 2.0 keV. Our calculations accurately capture the role of resonant excitation in Kr at 1.5 keV and Xe at 2.0 keV [9, 10] without resorting to a “superconfiguration” approach [30]. It is interesting to note that in order to produce the observed experimental yield above Xe³²⁺, the calculation needs to assume twice the experimental fluence [9]. Given the SASE XFEL beam profiles and the uncertainties of beam characterization, it is possible that a higher local fluence was present in the experiment.

To summarize, we have developed an efficient computational scheme that includes bound-bound resonant transitions to model ionization dynamics of atoms in intense, femtosecond XFEL pulses. Our MCRE scheme

uses effective atomic data storage and retrieval to track resonant excitations driven by the finite bandwidth pulse. We studied the response of atomic Ar in an intense 480-eV XFEL pulse and identified important ECs and pathways that lead to the production of high charge states of Ar. Furthermore, we accurately account for the role of resonant excitation in previously published Kr and Xe data. This work is the first theoretical verification of resonance-enhanced multiple ionization pathways (REXMI) and the method opens theoretical exploration of resonant high-intensity x-ray physics.

We thank Stephen Southworth, Robin Santra and Sang-Kil Son for their comments. This material is based upon work supported by the U.S. Department of Energy, Office of Science, Office of Basic Energy Sciences, under Contract No. DE-AC02-06CH11357. This research used resources of the Linac Coherent Light Source, which is a DOE Office of Science User Facility.

[1] P. Emma *et al.*, Nat. Photon. **4**, 641 (2010).
 [2] T. Ishikawa *et al.*, Nat. Photon. **6**, 540 (2012).
 [3] R. Neutze *et al.*, Nature **406**, 752 (2000).
 [4] H. N. Chapman *et al.*, Nature **470**, 73 (2011).
 [5] M. M. Seibert *et al.*, Nature **470**, 78 (2011).
 [6] L. Young *et al.*, Nature **466**, 56 (2010).
 [7] G. Doumy *et al.*, Phys. Rev. Lett. **106**, 083002 (2011).
 [8] E. P. Kanter *et al.*, Phys. Rev. Lett. **107**, 233001 (2011).
 [9] B. Rudek *et al.*, Nat. Photon. **6**, 858 (2012).
 [10] B. Rudek *et al.*, Phys. Rev. A **87**, 023413 (2013).
 [11] L. J. Frasinski *et al.*, Phys. Rev. Lett. **111**, 073002 (2013).
 [12] H. Fukuzawa *et al.*, Phys. Rev. Lett. **110**, 173005 (2013).
 [13] N. Rohringer and R. Santra, Phys. Rev. A **76**, 033416 (2007).
 [14] S.-K. Son and R. Santra, Phys. Rev. A **85**, 063415 (2012).
 [15] S. Schorb *et al.*, Phys. Rev. Lett. **108**, 233401 (2012).
 [16] E. V. Gryzlova *et al.*, Phys. Rev. A **84**, 063405 (2011).
 [17] Y. Hikosaka *et al.*, Phys. Rev. Lett. **105**, 133001 (2010).
 [18] Consider an atom with N active/accessible orbitals and g_j is the maximum occupation number of the active subshell j . Let C_k be the number of EC with a total number of k electrons in all active orbitals. In fact, C_k is the partition function for partitioning the integer k into N integers. In number theory, the generating function of C_k

is given by

$$\sum_k C_k x^k = (1-x)^{-N} \prod_{j=1}^N (1-x^{g_j+1}) \quad (2)$$

Then the total number of ECs with k_i to k_f is given by $\sum_{k=k_i}^{k=k_f} C_k$.

[19] W. Xiang *et al.*, Phys. Rev. A **86**, 061401(R) (2012).
 [20] A. A. Sytcheva *et al.*, Phys. Rev. A **85**, 023414 (2012).
 [21] S. Schorb, Ph. D. Thesis, (2012).
 [22] K. Motomura *et al.*, J. Phys. B: At. Mol. Opt. Phys. **46**, 164024 (2013).
 [23] C. P. Balla, N. O. Folland, and M. A. Hein, Phys. Rev. A **8**, 649 (1973).
 [24] S.-K. Son, L. Young, and R. Santra, Phys. Rev. A **83**, 033402 (2011).
 [25] R. P. Madden, D. L. Ederer, and K. Codling, Phys. Rev. **177**, 136 (1969).
 [26] H. Wang *et al.*, Phys. Rev. Lett. **105**, 143002 (2010).
 [27] The Sankey diagram is made using the “Sankey Diagram” package from Google Charts.
 [28] M. Hoener *et al.*, Phys. Rev. Lett. **104**, 253002 (2010).
 [29] B. Nagler *et al.*, Nat. Phys. **5**, 693 (2009).
 [30] O. Peyrusse, B. Deschaud, and D. Rolles, J. Phys. B: At. Mol. Opt. Phys. **47** 011001 (2014).